

Optoelectronic properties analysis of silicon light-emitting diode monolithically integrated in standard CMOS IC

Yanxu Chen(陈彦旭), Dongliang Xu(许栋梁), Kaikai Xu(徐开凯), Ning Zhang(张宁), Siyang Liu(刘斯扬), Jianming Zhao(赵建明), Qian Luo(罗谦), Lukas W. Snyman, Jacobus W. Swart
Citation: Chin. Phys. B . 2019, 28(10): 107801 . **doi:** 10.1088/1674-1056/28/10/107801
Journal homepage: http://cpb.iphy.ac.cn; http://iopscience.iop.org/cpb

What follows is a list of articles you may be interested in

Improvement of electro-optic performances in white organic light emitting diodes with color stability by buffer layer and multiple dopants structure

Zhi-Qi Kou(寇志起), Yu Tang(唐宇), Li-Ping Yang(杨丽萍), Fei-Yu Yang(杨飞宇), Wen-Jun Guo(郭文军)
Chin. Phys. B . 2018, 27(10): 107801 . **doi:** 10.1088/1674-1056/27/10/107801

Characteristic improvements of thin film AlGaInP red light emitting diodes on a metallic substrate

Bin Zhao(赵斌), Wei Hu(胡巍), Xian-Sheng Tang(唐先胜), Wen-Xue Huo(霍雯雪), Li-Li Han(韩丽丽), Ming-Long Zhao(赵明龙), Zi-Guang Ma(马紫光), Wen-Xin Wang(王文新), Hai-Qiang Jia(贾海强), Hong Chen(陈弘)
Chin. Phys. B . 2018, 27(4): 047803 . **doi:** 10.1088/1674-1056/27/4/047803

High color rendering index white organic light-emitting diode using levofloxacin as blue emitter

Miao Yan-Qin, Gao Zhi-Xiang, Zhang Ai-Qin, Li Yuan-Hao, Wang Hua, Jia Hu-Sheng, Liu Xu-Guang, Tsuboi Taiju
Chin. Phys. B . 2015, 24(5): 057802 . **doi:** 10.1088/1674-1056/24/5/057802

Improvement of electron injection of organic light-emitting devices by inserting a thin aluminum layer into cesium carbonate injection layer

Xin Li-Wen, Wu Xiao-Ming, Hua Yu-Lin, Xiao Zhi-Hui, Wang Li, Zhang Xin, Yin Shou-Gen
Chin. Phys. B . 2015, 24(3): 037802 . **doi:** 10.1088/1674-1056/24/3/037802

Effect of NaCl doped into Bphen layer on the performance of tandem organic light-emitting diodes

Xiao Zhi-Hui, Wu Xiao-Ming, Hua Yu-Lin, Bi Wen-Tao, Wang Li, Zhang Xin, Xin Li-Wen, Yin Shou-Gen
Chin. Phys. B . 2014, 23(8): 087811 . **doi:** 10.1088/1674-1056/23/8/087811

SPECIAL TOPIC — A celebration of the 100th birthday of Kun Huang

Optoelectronic properties analysis of silicon light-emitting diode monolithically integrated in standard CMOS IC*

Yanxu Chen(陈彦旭)[1], Dongliang Xu(许栋梁)[1], Kaikai Xu(徐开凯)[1,†], Ning Zhang(张宁)[1], Siyang Liu(刘斯扬)[2], Jianming Zhao(赵建明)[1], Qian Luo(罗谦)[1], Lukas W. Snyman[3], and Jacobus W. Swart[4]

[1] *State Key Laboratory of Electronic Thin Films and Integrated Devices, University of Electronic Science and Technology of China, Chengdu* 610054, *China*
[2] *National ASIC System Engineering Research Center, Southeast University, Nanjing* 210096, *China*
[3] *Department of Electrical Engineering, University of South Africa, Pretoria* 0001, *South Africa*
[4] *Faculty of Electrical and Computer Engineering, State University of Campinas – UNICAMP, Campinas CEP* 13083-852, *Brazil*

(Received 30 June 2019; revised manuscript received 24 August 2019; published online 28 August 2019)

Si p^+n junction diodes operating in the mode of avalanche breakdown are capable of emitting light in the visible range of 400–900 nm. In this study, to realize the switching speed in the GHz range, we present a transient model to shorten the carrier lifetime in the high electric field region by accumulating carriers in both p and n type regions. We also verify the optoelectronic characteristics by disclosing the related physical mechanisms behind the light emission phenomena. The emission of visible light by a monolithically integrated Si diode under the reverse bias is also discussed. The light is emitted as spatial sources by the defects located at the p–n junction of the reverse-biased diode. The influence of the defects on the electrical behavior is manifested as a current-dependent electroluminescence.

Keywords: silicon light-emitting diode, reverse bias, electro-optic modulation

PACS: 78.60.Fi, 73.61.Ey **DOI:** 10.1088/1674-1056/ab3e44

1. Introduction

Silicon-based optoelectronic integration technology as the cornerstone of future information technology has great potential in optoelectronic applications. However, this technology faces a bottleneck of lacking suitable silicon-based light source due to the silicon's indirect bandgap. To overcome this bottleneck, many silicon substrate light source schemes have been proposed.

In order to transform the indirect bandgap of silicon into direct bandgap, ultrathin Si_xGe_y strained layer super-lattices were proposed to fold the Brillouin zone.[1] Although new optical properties in terms of Si-based optical devices were developed, it is difficult to obtain a relatively low epitaxial dislocation density. The lifetime of phosphorescent organic light-emitting diodes (OLED) is usually poor due to the trap formed by triplet-polaron annihilation. The exciton distribution can be broadened and the exciton concentration can be reduced by using ultrathin light emitting layers (< 1 nm) and mixed bipolar interlayers.[2] The electro-optic performances and color stability can be further improved by changing the composition and the thickness of the buffer layer, which is in between the emitting and the electron transport layers.[3] Through adjusting the doping concentration of the quantum well barrier, a spectrum suitable for applications can be obtained. The effect of spectrum-control in dual-wavelength LED is due to the blocking effect of electrons and holes by doping quantum well barriers.[4] Nanocrystalline porous silicon receives much attention, in particular for its optoelectronic functions. Toward applications, there are two critical issues need to be highlighted: the luminescence quantum efficiency and its stability.[5,6] Erbium impurities are effective luminescence centers in silicon and exhibit sharp luminescence at 1.54 μm.[7,8] However, the Er-doped device faces the limitation of emitting intensity. Si quantum dots embedded in $SiO_x/SiN_x/SiC_x$ matrices are the key to overcome the shortcoming of poor emission efficiency in bulk Si.[9,10] Nevertheless, how to keep those embedded quantum dots stable is still a problem. In addition to Si based devices, deep-ultraviolet light emitting devices (DUVLEDs) also have a variety of potential applications. Zinc-oxide-based materials, which have wide bandgap and high exciton binding energy, have potential applications in high-performance DUVLEDs. To realize such optoelectronic devices, the modulation of the bandgap is required.[11]

Light emission from silicon devices has been realized in reverse-biased p–n avalanche structures.[12] High speed is required in optical interconnects, and GHz modulation bandwidth will limit the applications of this technology.[13] The purpose of this paper is to present our efforts on searching for the high speed of a silicon p–n junction switching of light emission.

In this study, the avalanche impact ionization process is presented to evaluate the emitted photons. The operational

*Project supported by the National Natural Science Foundation of China (Grant No. 61704019).
†Corresponding author. E-mail: kaikaix@uestc.edu.cn
© 2019 Chinese Physical Society and IOP Publishing Ltd

speed of avalanche breakdown mode is determined by the *RC* time constant of the device, as well as the carrier transit time through the depletion region.[12] Our study suggests that the device working under avalanche breakdown mode has a potential to reach gigabit rates.

2. Device fabrication

The proposed Si optoelectronic device structure is realized on a Si substrate by using typical silicon CMOS process technology. Starting from a 1-μm-thick n-type ⟨100⟩ silicon layer, an active region with p-type heavy doping is deposited on the surface through standard lithography and wet etching techniques. The device described in this paper has a width of 175.5 μm and a length of 6 μm, and the cross-sectional view is schematically given in Fig. 1.

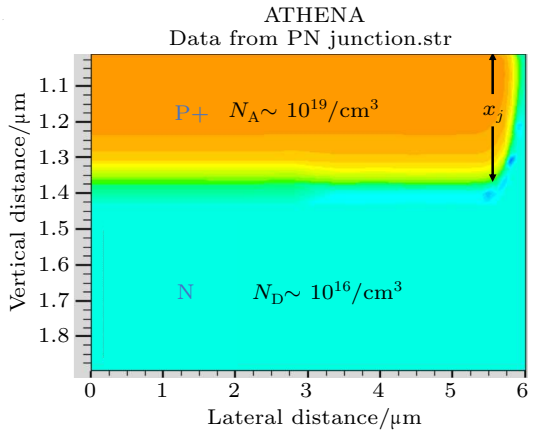


Fig. 1. Cross-sectional view of the Si optoelectronic device structure.

3. Structural and optical properties of the device

As the reverse bias of the p–n junction increases, electrons and holes are accelerated to attain enough energy in the avalanching region with high electric field. When the reverse bias causes junction breakdown, newly generated electron-hole pairs collide with the lattice and transfer energy to realize light emission. Indeed, both electrons and holes are excited in the related excitation zone in the avalanching junction. Hot electrons may recombine with hot holes in the excitation zone,[14] contributing to photons emitted from the high-field region in the avalanching p$^+$n junction shown in Fig. 2.

The avalanche breakdown voltage (BV) is numerically calculated using the background doping dependent model given as[15]

$$BV = \frac{9b^2/(4qN_D/\varepsilon_{si})}{\left\{\ln\left[\frac{V^{3/2}\pi a^2}{b(qN_D/\varepsilon_{si})^{1/2}}\mathrm{erf_c}^2\left(\frac{\sqrt{b}}{2(qN_DV_{BV}/\varepsilon_{si})^{1/4}}\right)\right]\right\}^2}, \tag{1}$$

where a and b are constants related to the breakdown, q is the electron charge, and V is the voltage of reverse bias; N_D is doping concentration of the substrate, and ε_{si} is the dielectricity of silicon. Accordingly, the p–n junctions BV is ~ 30 V for a 10^{16} cm^{-3} background doping concentration.

Tam and Hu measured the difference between the temperature dependence of the driving current and the temperature dependence of the photon-induced current.[16] The photon energy emitted from the reverse-biased p–n junction can be investigated by a dependence of hot-carrier effects on electron temperature. Accordingly, the photon energy intensity distribution function is given as

$$f(E) = c \cdot \exp(-E/kT_e), \tag{2}$$

where c is a constant, k is the Boltzmann's constant, E is the energy of photon, and T_e is the effective temperature of the hot carrier.[17]

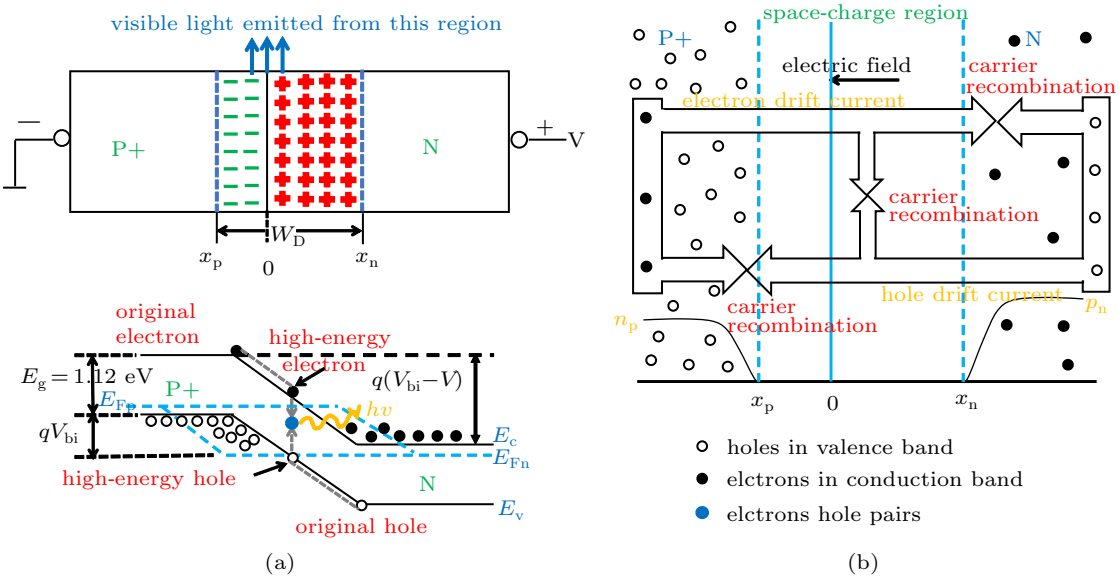


Fig. 2. Schematic photon emission phenomena in Si avalanching junction.

As shown in Fig. 3(a), when the reverse bias is over 30 V, the p–n junction starts to have avalanching breakdown, where the electric field peak surpasses 1.6×10^5 V/cm. The depletion width becomes wider slightly with the increase in the reverse biased voltage. Since the increase of the electric field is almost uniform, the relationship between the field's maximum and the reverse bias voltage is very close to a linear dependence, as depicted in Fig. 3(b).

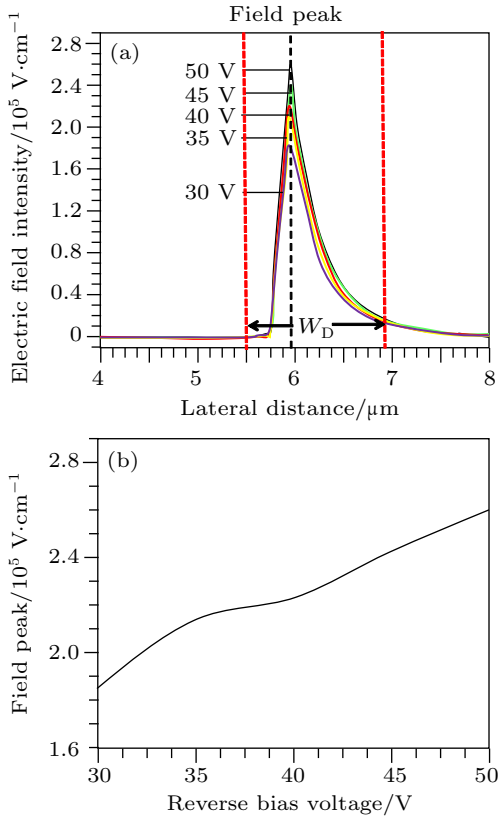


Fig. 3. Characterization of the depletion region: (a) simulated electric field distribution in the drift region obtained through Poisson equation integration; (b) field peak as a function of reverse biased voltage.

The process of filament formation sets an upper limit to the light modulation speed. The filament formation time is typically governed by the transit time of the carriers reaching the depletion edge of the p–n junction. And it is given as

$$t = W_D/v, \tag{3}$$

where W_D is the depletion width and v is the saturated drift velocity of the electrons. For a breakdown voltage of 30 V, the depletion width of the junction under the reverse bias is approximately 1.4 μm and the saturated drift velocity is 10^7 cm/s, resulting in the theoretical limit of light modulation at ∼ 14 ps. For more luminous wider junctions having larger breakdown voltage, the time required for filament formation is longer (about a few hundred picoseconds), limiting the speed of light emission lower than 10 GHz.[18] In this case, the corresponding speed for the specific p–n junction diode is $f_t = 1/(2\pi t) = 11$ GHz.

The capacitance in the structure of p–n junction diodes is another way to investigate the transient characteristics of the p–n junction structure-based silicon light source. The capacitance in the structure is defined in Fig. 4, in which there is a capacitance associated with the depletion layer of the diode. As the diode is switched from off (zero-biased or reverse-biased) to on (forward-biased), it takes some time before the diode is turned on and reaches the steady state. This time is associated with charging up the depletion-layer capacitor and filling up the p- and n-regions with excess minority carriers. Similarly, when a diode is switched from the on state to the off state, it also takes some time before the diode is turned off. This time is associated with discharging the depletion-layer capacitors and discharging the excess minority carriers stored in the p-and n-regions. The majority-carrier response time, or the dielectric relaxation time, is much shorter, on the order of 10 ps.

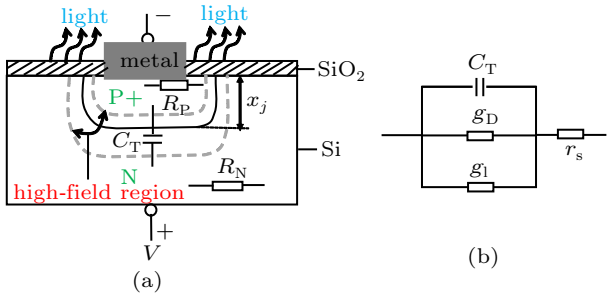


Fig. 4. Capacitance in a p–n junction diode structure: (a) schematic view; (b) equivalent circuits of a p–n junction capacitor.

Time is needed to charge and discharge the depletion-layer capacitor. The depletion-layer capacitance C_T as shown in Fig. 4 is typically on the order of 1 fF/μm^2. When the diode is operated, the current density J is of 1 mA/μm^2. Then the time associated with charging and discharging the depletion-layer capacitor is of the order of $C_T V/J$, which is of the order of 10 ps. Of course, this time changes in proportion to the current density J. However, as we will show below, the time needed to charge or discharge the depletion-layer capacitor is usually very short compared with the time associated with charging or discharging the p- and n-regions of their majority carriers. In addition, in Fig. 4, g_D denotes the p$^+$n junction's transconductance under DC condition, g_l is the intrinsic transconductance related to the junction's leakage current, depending on the device fabrication process, and r_s is the resistance (which is mainly consisted of the sheet resistance of the p-type and n-type layers in Fig. 1).

Since the cross section's area of the junction is $W \times L =$ 175.5 μm × 6 μm, the total capacitance $C = C_T \times (WL)$ is of the order of 10^{-16} F. The capacitance C_T of the silicon p$^+$n junction diode under the reverse-bias was simulated using the device simulator MEDICI[19] to understand the transient nature of electro-optic modulation.[20] As shown in Fig. 5, the simulated depletion capacitance is plotted as a function of

junction's reverse bias voltage. The capacitance of the p–n junction based silicon light source decreases with the driving voltage when the device is turned on to avalanche breakdown. Stronger recombination in the luminescence active region induces negative capacitance phenomena.[21]

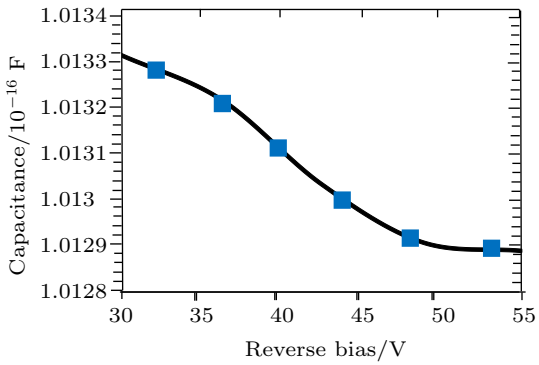


Fig. 5. Parasitic capacitance–voltage characteristic of the silicon light-emitting device with p–n junction structure.

The forward-biased operation of p–n junctions for light emission is a slow, inefficient, and unreliable process because of the lifetime of the minority carriers. Any attempt to increase the speed of operation by removing the minority carriers reduces the efficiency of light emission.[18] The dynamic on-resistance of the p–n junction in avalanche is in the tens of kΩ range and the reverse-biased junction capacitance is in the range of pF. Then the *RC* time constant will be in the range of tens of ps. This will be sufficient to produce modulation in excess of 10 GHz.[22] Both the carrier lifetime depending on the electric field model and the capacitor's discharging time depending on the *RC* time constant verify that a combined switching speed in the range of 10 GHz may still attainable for the p–n junction carrier injection light-emitting device in silicon devices.[12]

In avalanche mode, the electron–hole pairs can be accelerated by the electric field as well as gain excess energy. Those pairs could recombine radiatively. Figure 6 shows the silicon band structure model processes. The mechanisms of this recombination are as follows: hot electrons and holes recombine band-to-band, bremsstrahlung of the electrons corresponding to transitions within the conduction band and recombination of holes in the valence band.[20] As shown in Fig. 7, spectroscopic measurements of the emitted light reveal clear emission peaks at 1.75 eV and 2.07 eV in the 400–900 nm wavelength region. In general, the mechanism of indirect interband transitions of energetic electrons in the conduction band and holes in the valence band is for low photon energy levels. Bremsstrahlung radiation is suggested for interpreting the intermediate photon energy level, and direct and indirect interband recombination contributions for high photon energy levels. The mechanisms of recombination could explain why those main radiation wavelength peaks are not close to the bandgap.

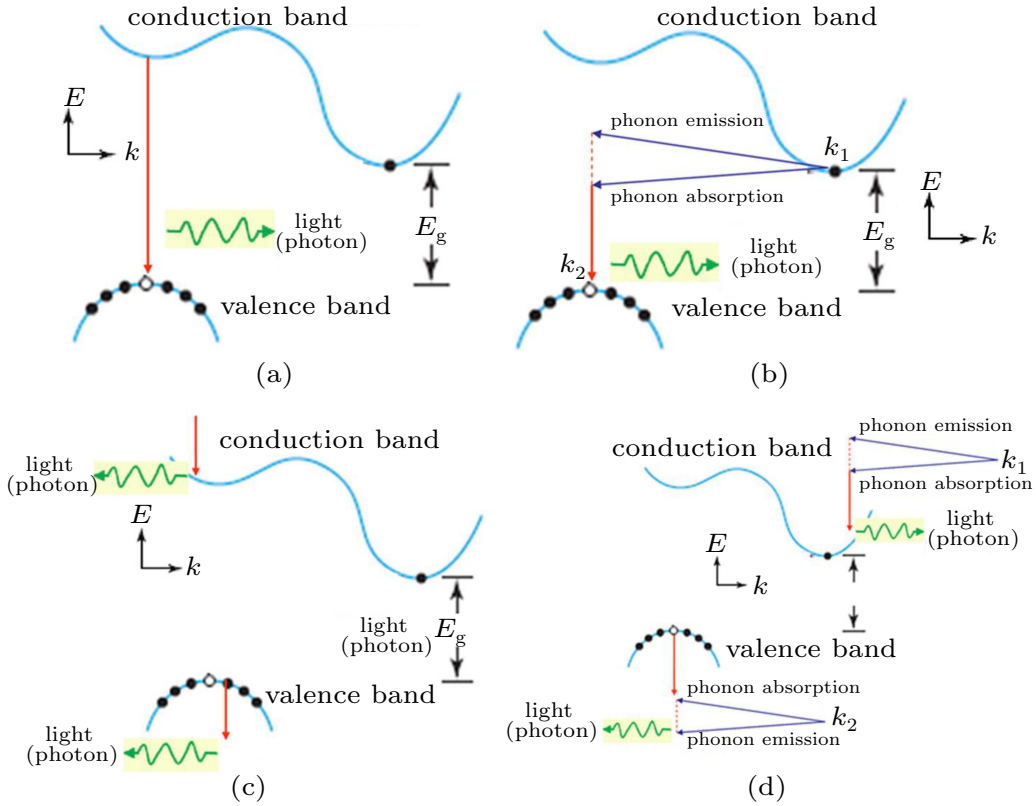


Fig. 6. Possible photonic energy transitions in the silicon band diagram: (a) direct-interband transition, (b) indirect-interband transition, (c) direct-intraband transition, and (d) indirect-intraband transition.

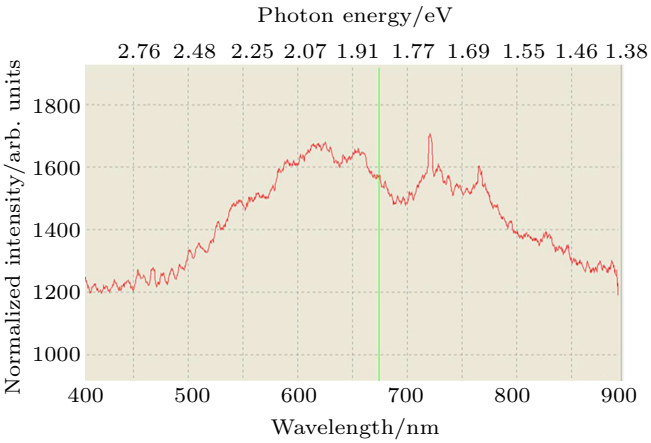


Fig. 7. Intensity spectra of the p–n junction based silicon light-emitting device in the injection-avalanche mode of operation for various injection current levels (in this case a reverse current of 45 mA induced by the junction's avalanching is applied).

We measured the emission power from the Si p^+n junction device by using a calibrated power meter. The external quantum efficiency η_Q, which describes the conversion of carriers into photons, can be written as

$$\eta_Q = \left(\frac{P}{hc/\lambda}\right) / \left(\frac{I}{q}\right). \tag{4}$$

Here, q is the elementary charge, λ is the wavelength, h is the Planck constant, c is the speed of light, and I is the reverse current. The power conversion efficiency η_P is defined as

$$\eta_P = \frac{P}{I \times V}, \tag{5}$$

where V is the reverse bias voltage, P is the externally measured optical output power, and $I \times V$ is the current–voltage product which means the applied total electrical power. By substituting Eq. (5) into Eq. (4), the relationship between the quantum efficiency and the power conversion efficiency can be derived as

$$\eta_Q = (qV\lambda/hc)\eta_P. \tag{6}$$

The emission efficiency is presented in Fig. 8.[23]

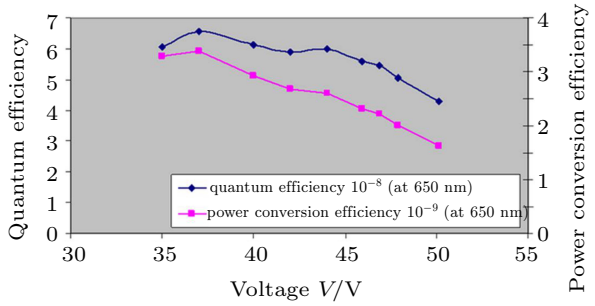


Fig. 8. Efficiency of Si p^+n junction. For instance, at the reverse bias $V = 40$ V, the quantum efficiency (blue diamonds) is about 6×10^{-8} and the power conversion efficiency (pink squares) is 2.8×10^{-9}.

Manufacturing these photonic devices is still a challenge. The processing starting with the same silicon wafers in microelectronics has been ubiquitous for decades. Optical components and circuitry onto wafers alongside the microelectronic elements have been introduced using many manufacturing tools in standard semiconductor fabs. However, because photons fundamentally do not obey the same physics as electrons, guiding a photon from one element to another inside a packaged chip is not as simple as soldering the two together. Thus alignment tolerances are much more exacting. Whereas connecting a wire to a contact-pad on a chip involves aligning the components to within a few tens of micrometres of the correct position, connecting an optical fibre to a photonic chip can require three orders of magnitude more precision. Fortunately, thanks to ingenious device engineering and some groundbreaking micro-robotic industrial automation technology, we are well on our way to overcoming these challenges, bringing high-throughput photonic interconnects into the mainstream.

4. Conclusion and perspectives

A transient model to establish a relationship of light emission from avalanche breakdown in Si p–n junctions with the applied reverse bias voltage is demonstrated. Theoretical simulations and experimental measurements of the capacitances and series resistances indicate that the device has an intrinsic high-frequency operating capability in the near gigahertz range. The spectral radiance as a function of wavelength is also shown, which reveals clear high intensity peaks at about 625 nm and 725 nm. A compatible CMOS technology light-emitting device is proposed with an optical output of several nW. Hence, some interesting chip-to-chip and on-chip electro-optical applications seem feasible in the next-generation VLSI integrated circuitry.

Acknowledgment

The authors thank Prof. Ian White of the University of Cambridge for useful suggestions.

References

[1] Presting H, Kibbel H, Jaros M, Turton R M, Mencrigar U, Abstreiter G and Grimmeiss H G 1992 *Semicond. Scl. Technol.* **7** 1127
[2] Jian Y, Nan Y and Dong D 2019 *Acta Phys. Sin.* **68** 017202 (in Chinese)
[3] Kou Z, Tang Y and Yang L 2018 *Chin. Phys. B* **27** 107801
[4] Liu X, Fan G and Zhang Y 2012 *Acta Phys. Sin.* **61** 138503 (in Chinese)
[5] Lu Y, Shi Z and Shan C 2017 *Chin. Phys. B* **26** 047703
[6] Tsybeskov L 1998 *MRS Bull.* **23** 33
[7] Gelloz B, Kojima A and Koshida N 2005 *Appl. Phys. Lett.* **87** 031107
[8] Priolo F, Coffa S, Polman A and Carnera A 1994 *Appl. Phys. Lett.* **64** 2235
[9] Benton J L, Michel J, Kimerling L C, Jacobson D C, Xie Y H, Eaglesham D J, Fitzgerald E A and Poate J M 1991 *J. Appl. Phys.* **70** 2667
[10] Cheng C H, Lien Y C, Wu C L and Lin G R 2013 *Opt. Express* **21** 391
[11] Tai H Y, Lin Y H and Lin G R 2013 *IEEE Phot. J.* **5** 6600110

[12] Snyman L, Du Plessis M and Bellotti E 2010 *IEEE J. Quantum Electron.* **46** 906
[13] Xu K, Snyman L and Aharoni H 2017 *Opt. Mater.* **69** 274
[14] Snyman L, Du Plessis M and Aharoni H 2007 *J. Appl. Phys.* **46** 2474
[15] Ma P, Linder M, Sanden M, Zhang S L , Östling M and Chang M C F 2001 *Solid Stat. Electron.* **45** 159
[16] Tam S and Hu C 1984 *IEEE Trans. Electron. Dev.* **31** 1264
[17] Du Plessis M, Wen H and Bellotti E 2015 *Opt. Express* **23** 12605
[18] Chatterjee A, Bhuva B and Schrimpf R 2004 *IEEE Electron Device Lett.* **25** 628
[19] MEDICI 2010 *Technology Modeling Associates* (Palo Alto, CA)
[20] Xu K, Liu S, Zhao J, Sun W and Li G 2015 *Opt. Eng.* **54** 057104
[21] Wang C, Zhu C, Zhang G, Shen J and Li L 2003 *IEEE Trans. Electron. Dev* **50** 1145
[22] Chatterjee A and Bhuva B 2003 *Solid-State Electron.* **47** 665
[23] Xu K, Zhang Z and Zhang Z 2016 *J. Nanophoton.* **10** 016002